
Intruder mobility in a vibrated granular packing

RIM HARICH, THIERRY DARNIGE, EVELYNE KOLB, ERIC CLÉMENT

Laboratoire de Physique et Mécanique des Milieux Hétérogènes (UMR 7636 et Universités Paris 6 et Paris 7), 10 rue Vauquelin, 75005 Paris, France

PACS 47.70.-n – Granular systems

PACS 45.70.Mg – Granular flow

Abstract. - We study experimentally the dynamics of a dense intruder sinking under gravity inside a vibrated $2D$ granular packing. The surrounding flow patterns are characterized and the falling trajectories are interpreted in terms of an effective friction coefficient related to the intruder mean descent velocity (flow rules). At higher confining pressures i.e. close to jamming, a transition to intermittent dynamics is evidenced and displays anomalous "on-off" blockade statistics. A systematic analysis of the flow rules, obtained for different intruder sizes, either in the flowing regime or averaged over the flowing and blockade regimes, strongly suggest the existence of non-local properties for the vibrated packing rheology.

Introduction. – During the last decades, several studies have shown amazing analogies among variety of very different systems [1] (colloids [2], foams [3], granular materials [4,5], supercooled liquids [18]). Indeed, close to the jamming transition these systems share common dynamical behaviors such as a glassy phase, aging, memory or intermittency [6]. Based on these analogies, several propositions emerged aiming to describe and possibly understand, in a general and unified way, this phenomenology and the associated rheology [7,8]. In the case of dense granular packing, the rheology under shear is described with good accuracy by local relations between a dynamical friction coefficient and a local dimensionless number, involving shear and confining pressure [4]: the inertial number. However, the boundary between fluid-like and solid-like phases is still poorly understood. Experiments on avalanche flows suggest that the rheology could indeed be non-local near arrest [9,10]. Conceptually, for the rheology of vibrated granular packing, the most elaborated point of view stems from kinetics theory [11]. Whereas this simple vision is reliable to describe dilute systems, it is severely challenged for dense systems [15–17,29]. It has been suggested in this case, that the notion of thermal temperature could be replaced by the more general concept of "effective temperature" describing the structural evolution between blocked configurations [12]; however, practically, it is quite difficult to apply this concept in order to obtain a clear constitutive picture. In experiments, a complication usually comes from the way energy is input in the packing

i.e. from the boundaries. It often leads to very inhomogeneous bulk agitations, both in time and space. The probes themselves are hard to decouple from the agitation energy input [13,14], which may alterate the reliability of the constitutive relations hence extracted [14]. This was somehow circumvented recently by Reis et al. [15] and Lechenault et al. [16], who studied $2D$ horizontal packing driven homogeneously from the bottom; same for Keys et al. [17] using an hydrodynamic fluidization technique. In these experiments, which approach jamming by increasing the packing compaction, strongly heterogeneous and cooperative displacement modes were evidenced, very reminiscent to those present in undercooled liquids or glassy systems [18].

Recently, Caballero et al. [19] studied a sonofluidized $3D$ granular packing and monitored the motion of various intruders inside. Even at weak driving acceleration, the resulting friction coefficients decrease significantly with acceleration. Eventually, the Coulomb threshold vanishes and one obtains a linear relation between force and velocity. These relations are strongly dependent on the shape and the size of the intruders. Other means of activation were proposed using shear bands noise as actuators [20,21]. In these last cases, empirical relations between force and velocity were extracted and all these works concluded on the non-local character of the constitutive relations. However, in all these cases, the intruder was buried partially or completely in the bulk, thus hindering a direct visualization of granular motion in the intruder surrounding.

In the present work, we seek to extract the rheological properties of a vibrated vertical granular packing by monitoring the vertical motion of cylindrical intruders. This approach is very analogous to bead rheometers techniques currently used in fluid mechanics. Note also some recent work along those lines on intruder penetration in 2D or 3D packing but in the absence of vibration [25, 26]. This kind of experiments were also performed in other systems like colloids [2], glasses [24] or foams [27].

The paper is organized as follows. First, we present the experimental setup, a 2D experiment realization of a vibrated granular packing oriented in the direction of the gravity. Then, the descent dynamics of heavy intruders are monitored in association with the resulting counterflow of the surrounding particles. We show that the analysis of the intruder trajectories may probe a rheological behavior via a relation between an effective friction coefficient and the mean intruder descent velocity. We analyze the intermittent statistics evidenced at higher depths as an alternation of flow and blockade. We finally question the existence of a local relationship accounting for the rheology of the dense granular medium under vibration.

Set-up and experimental protocol. – Figure 1(a) displays a snapshot of the experimental set-up. The cell is a vertical rectangular container of lateral size $L = 275$ mm and thickness 3.5 mm slightly larger than the thickness of the disks forming the model granular packing. We use a bi-disperse mixture of around 1100 big (diameter $d_b = 5$ mm) and 1600 small (diameter $d_s = 4$ mm) nylon disks of thickness 3 mm. The intruder is a metallic cylinder of adjustable radius R and same thickness as the grains. The average intruder density can also be adjusted by drilling a hole at its center. The density contrast with the surrounding vibrated granular medium of density ρ is defined as $\frac{\Delta\rho}{\rho}$ and is always chosen positive. Therefore, the intruder will sink due to buoyancy if the surrounding medium is fluidized enough.

The way vibration energy is input in the system, differs from what has been done in previous experiments. Here, we seek to avoid synchronization between the global motion of the packing and the sinusoidal motion of the driving plate. It is known that for accelerations larger and around gravity g , the packing trajectory and the energy input due to repetitive collisions with the bottom plate, are strongly synchronized, unless a very high acceleration level is reached (up to $30g!$ [28]). Note also that for driving accelerations larger than g , surface instabilities such as Faraday waves may also occur which render the packing spatially inhomogeneous [30]. Here, the idea is to break as much as possible this spatio-temporal synchronisation responsible for the alternation of phases at drastically different agitation levels. To this purpose, we place a so-called "vibrating chain" at the bottom of the cell (see Figure 1(a) bottom) which consists of two arrays of large and dense disks activated from below by 24 electromagnetic pistons oscillating vertically with an amplitude

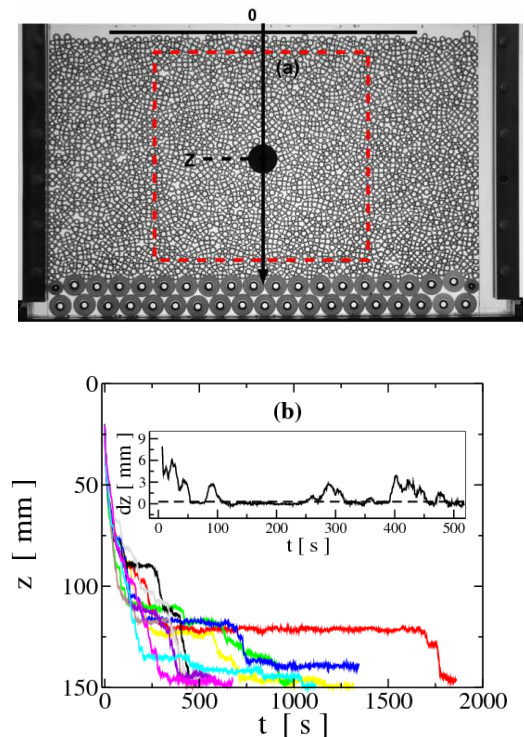


Fig. 1: (a) View of the cell containing the bi-disperse packing and a cylindrical intruder of radius $R = 10$ mm with $\rho \simeq 0.62 \text{ g.cm}^{-3}$. The dashed rectangle is the visualization field. (b) Vertical positions of the intruder as a function of time for 10 experiments with identical conditions of vibrations (radius $R = 10$ mm, density contrast $\frac{\Delta\rho}{\rho} = 16.15$). Inset : vertical increment of displacement for a time lag 1s for one of the intruder trajectories presented in the main graph (same color).

A_p inside the granular packing and thus, transferring vibration energy to this "chain". A detailed study of bulk agitation and packing density hence obtained at steady-state, is discussed elsewhere [31].

In this report, the packing is vibrated under fixed driving conditions : piston amplitude $A_p = 6$ mm and driving frequency $f_D = 20$ Hz with a phase shift of π between neighboring pistons. We measured for this system a driving RMS acceleration of $2g$ in the vertical direction. In a typical experiment, the vibration is activated 15 minutes before we place the intruder at the piling surface. Its descent is monitored by a CCD camera taking pictures every second. For each intruder we perform 10 experiments in similar experimental conditions.

Intruder descent dynamics. – Figure 1(b) shows the vertical positions $z(t)$ of an intruder of radius $R = 10$ mm as a function of time. The first noticeable feature is that the intruder motion is quite irregular with alternate phases of flow and blockade. The deeper the intruder is in the packing, the more likely blockade seems to occur (see inset of figure 1(b)). This intermittent dynamics yields a

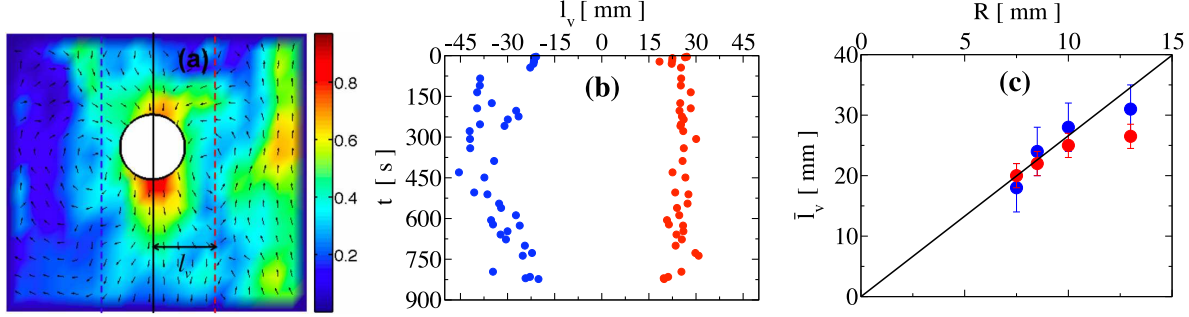


Fig. 2: (a) Average displacement field for a time lag corresponding to an intruder displacement over its radius $R = 10$ mm and for a coarse-graining size $\Delta W = d_s$. The color code represents the amplitude of the coarse-grained displacement normalized by the intruder radius and the vectors indicate the direction of grain motion. Note the horizontal distance l_v between the intruder center and a vortex center. (b) Horizontal positions of left and right vortex centers as a function of time (density contrast $\frac{\Delta\rho}{\rho} = 16.15$), (••) right vortex and (•) left vortex. (c) Mean horizontal distances \bar{l}_v between the intruder and the vortex centers as a function of the radius R (symbol colors as in (b)).

large distribution of arrival times at the bottom of the cell as observed from the different vertical trajectories taken in identical conditions.

Figure 2(a) displays the coarse-grained displacement field over a time lag τ defined using the mean intruder sinking time over a distance R . A feature of these displacement fields is the existence of two vortices accompanying the intruder's descent and corresponding to recirculations of grains around the intruder. Note that during a descent, one of the vortices seems to be dominant in amplitude but it can be located on either side of the intruder. In figure 2(b), the distances l_v joining the intruder's center to both vortex centers are represented as a function of time. From Figure 2(b), we see that during the whole fall both vortices seemed to stay at a fixed distance $\bar{l}_v(R)$ from the intruder. We thus represented this mean distance $\bar{l}_v(R)$ for experiments done with different intruder sizes and observed that these distances scale almost linearly with the radius R (Fig. 2(c)).

Effective friction. – One objective of this study is to shed light on the rheological properties of granular matter under vibration. In either static, quasi-static or dense flow situations, the central constitutive parameter describing the granular rheology is the ratio μ between shear stress and confining pressure (see [4] and refs. inside), i.e., a Coulomb friction coefficient. Scaling analysis shows that for an intruder of radius R , the driving force per unit of thickness F_G is set by gravity, thus $F_G \propto \Delta\rho g R^2$. This force must be balanced at steady state by the resulting friction force exerted on the intruder boundary $F_S \propto \mu \rho g z R$. Thus, a relation can be obtained for the friction coefficient μ which scales like $\mu \propto \Delta\rho R / \rho z$, where $\frac{\Delta\rho}{\rho}$ is the density contrast, R the intruder radius and z its vertical depth. This argument can be made more quantitative in the framework of a simple reference model involving a constant dynamical friction μ so that effective friction

and dynamical friction would match ($\mu_e = \mu$). The force balance can be computed exactly by considering a local confining pressure imposed by gravity $P = \rho g z$ and by integrating the friction force around the intruder. This is the base for our definition of an effective friction coefficient μ_e :

$$\mu_e = \frac{\pi \Delta\rho R}{4 \rho z} \quad (1)$$

This relation motivates a parametric study of the intruder motion by varying its size and its apparent density. For each realization i , we measure the time $\tau_i(z)$ spent by the intruder to span the interval $[z - \Delta z/2, z + \Delta z/2]$. Then, the mean descent velocity is defined as $\bar{V}(z) = \langle \Delta z / \tau_i(z) \rangle_i$, the average being taken over 10 realizations.

Dimensionless number. – In figure 3(a), we display for an intruder of radius $R = 10$ mm, the mean descent velocity $\bar{V}(z)$ obtained for $\Delta z = 20$ mm and for different density contrasts. As expected the mean velocity increases with density contrast. We also note the very regular decrease of mean velocity with depth z . In order to rescale the different curves, we define for each depth (z), a local mean Froude number as $\bar{Fr} = \bar{V} / \sqrt{P/\rho} = \bar{V} / \sqrt{g z}$. In Figure 3(b), we observe a rescaling of all the data on a common flow rule, which justifies the existence of an effective friction coefficient describing the rheology of the granular intrusion. Interestingly, this flow rule is of the hardening type, i.e., the effective friction increases with the local drag velocity, a behavior also observed for sheared dense granular media [4] without [26] or with vibration [19–21].

Blockade and flow statistics. – We previously noticed (see Figure 1(b)) that a prominent feature of the intruder descent dynamics is the intermittent sequel of blockades and flows. This clearly has a strong impact on the effective mean velocity as measured previously. In the

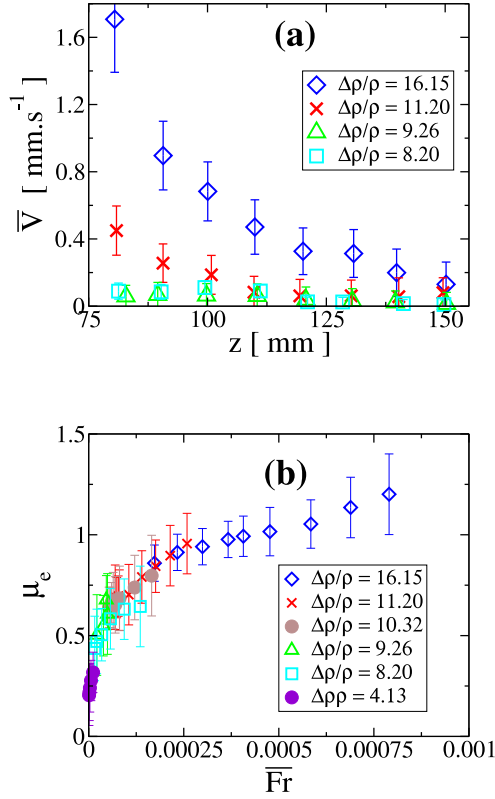


Fig. 3: (a) Mean velocity $\bar{V}(z)$ as a function of depth $z \pm \Delta z/2$ with $\Delta z = 20$ mm and for $R = 10$ mm and different density contrasts $\frac{\Delta\rho}{\rho}$. (b) Effective friction $\mu_e(z)$ as a function of Froude number $\bar{Fr}(z) = \frac{\bar{V}}{\sqrt{P/\rho}}$ for different density contrasts.

following, we will seek to separate and characterize both regimes independently. The method we design to extract the blocked phases is based on the use of a displacement threshold δ_Z at a time scale $\delta t = 1$ s below which we consider the intruder is blocked (see the dashed line in inset of figure 1(b)). This choice is somehow arbitrary; however, we rationalized it by defining, for each descent curve, a value such that the jump distribution in the blocked phase is close to a symmetric Gaussian curve with a zero average. For each trajectory, we identify the depths at which the intruder gets blocked and starts flowing again as well as the time spent in both phases respectively. Figure 4 displays the distribution of times spent in the blocked phase t_b at different depth values ($z \pm \Delta z/2$). The striking feature is the outcome of a power-law distribution $t^{-\alpha}$, with an exponent smaller than 2 ($\alpha \cong 1.5$). Such a distribution is the sign of an anomalous statistics as no typical time scale can be defined. To characterize the sojourn in the blocked phase, we thus consider the fraction of time Φ_b spent in the blocked phase at different depths.

In figure 5, Φ_b is plotted as a function of the effective

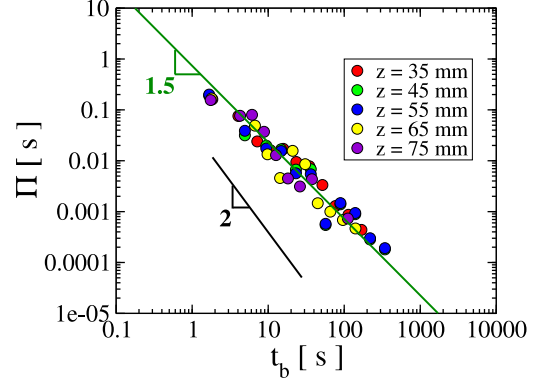


Fig. 4: Probability density function of blockade times $\Pi(t_b)$ for $R = 10$ mm and $\frac{\Delta\rho}{\rho} = 16.15$, at different depths.

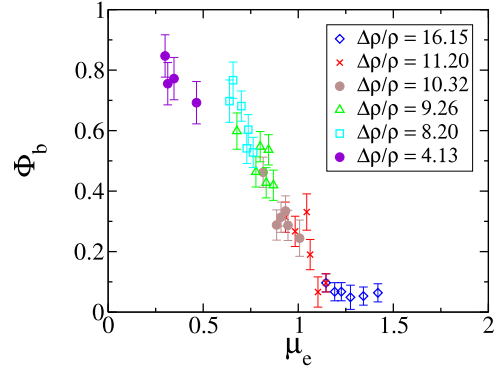


Fig. 5: Fraction of time $\Phi_b(z)$ spent in the blocked phase as a function of the effective friction $\mu_e(z)$ for $R = 10$ mm and different density contrasts $\frac{\Delta\rho}{\rho}$.

friction $\mu_e(z)$. At low μ_e , Φ_b is large and almost constant. At $\mu_e \cong 0.7$ a sharp decrease of the fraction of blocked time is observed. This transition from blockade to flow suggests a generalization of the static Coulomb threshold in the presence of vibration. Note that this effect of threshold distribution was also evidenced in numerical simulations of sheared granular packings under random noise [29].

Now we want to characterize the flowing phases. We define a flowing time variable t_F by removing *sequentially* the blockade periods of the trajectories. Figure 6(a) displays the flowing trajectories i.e. the intruder positions as a function of t_F . A clear collapse of all the trajectories is observed and an average is performed over 10 experiments done in identical conditions in order to define a mean flowing trajectory $z(t_F)$. A flowing velocity is then computed at each depth $\bar{V}_F = \frac{dz}{dt_F}$. This procedure allows to define a new Froude number $\bar{Fr}_F = \frac{\bar{V}_F}{\sqrt{P/\rho}}$, (with the subscript F for flow) that we call the dynamical Froude number as it applies to the flowing phase only.

In figure 6(b), we display the relation $\mu_e(\bar{F}r_F)$ for an intruder of radius $R = 10$ mm and for various density contrasts. Interestingly, we also observe a data collapse onto a unique curve.

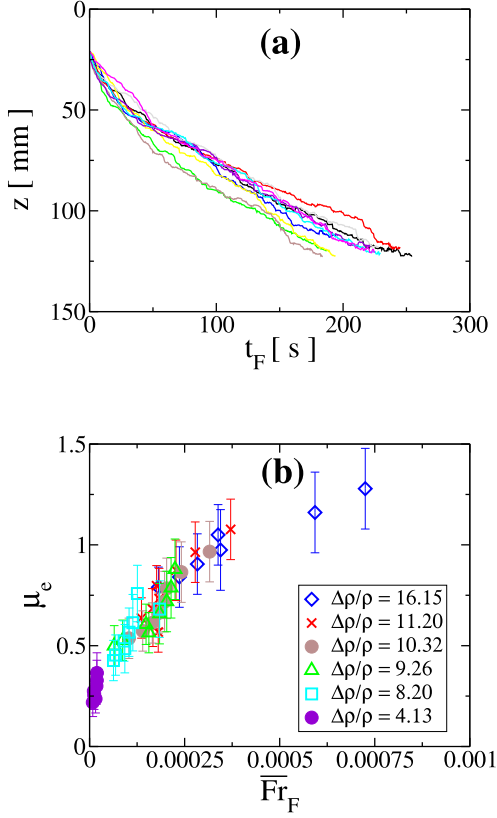


Fig. 6: (a) Vertical positions z of the intruder with $R = 10$ mm corresponding to fig.1(b), as a function of the flowing time variable t_F . (b) Dynamical flow rule : effective friction $\mu_e(z)$ as a function of the dynamical Froude number $\bar{F}r_F(z) = \frac{\bar{V}_F(z)}{\sqrt{g\bar{z}}}$ for various density contrasts $\frac{\Delta\rho}{\rho}$.

Towards a non-local rheology ?. – To extract a local rheology that could reflect constitutive properties of granular matter under vibration, we must at the end, provide a relation between a constitutive coefficient (friction) and local macroscopic fields such as pressure or shear rate and this, independently of the intruder’s presence. To address explicitly this question, we computed systematically the mean and dynamical flow rules corresponding to intruders whose diameter varies between 3.75 and 6.5 small granular sizes d_s . We obtained in each case - like what was presented previously for $R = 10$ mm - a rescaling of the data with different density contrasts. By visualization of the intruder flows (see Figures 2(a) and (b)), we have seen that shear is exerted on the intruder side at a distance of the order of $l_v(R)$ yielding a typical shear rate $\dot{\gamma} \cong \frac{\bar{V}}{l_v(R)}$. Following the analysis provided for rapid dense flows, we may try to transform the flow

rules into a local rheology law using an inertial parameter $I = \frac{\dot{\gamma}d_s}{\sqrt{P/\rho}} = \frac{d_s\bar{V}(z)}{l_v\sqrt{g\bar{z}}} = \frac{d_s}{l_v}\bar{F}r$. If a local rheology applies, a relation $\mu_e(I)$ should show up independently of the intruder size. We see in Figures 7(a) and (b) that the flow rules for different intruder’s size can be rescaled by dividing the Froude numbers by a value $\bar{F}r^*(R)$ for the mean flow rule or $\bar{F}r_F^*(R)$ for the dynamical flow rule. These rescaling values are presented as a function of the intruder radius R in insets of Figures 7(a) and (b). However, we observed that for both flow rules the corresponding lengths $\bar{F}r^*(R)d_s$ and $\bar{F}r_F^*(R)d_s$, grow much faster with R than $l_v(R)$. Therefore these rescalings could not provide a value such that the Froude ratios could be identified with an inertial parameter independent of R . Thus, it becomes clear that contrarily to the situation of rapid dense flows, the flow rule cannot be transformed into a local rheology using an inertial parameter. Whether this is the sign of true non-locality in the constitutive relations associated with a growing length scale near jamming or the unravelled influence of a supplementary field such as ”fluidity” or ”granular temperature” is left for future discussions. Note finally that under constant velocity and confining pressure, the effective friction increases when the intruder size decreases. This is the so-called ”geometrical hardening” effect already noticed by Caballero et al. [19].

Conclusion. – In this experimental study, we measured the dynamics of dense intruders sinking in a vibrated granular packing. The flow fields around the intruder was measured and characterized by two side vortices accompanying the intruder’s descent. The mean position of these vortices scales with the intruder size. The sinking dynamics is interpreted as an effective friction coefficient increasing with the mean falling velocity. For a given intruder size, when the mean falling velocity $\bar{V}(z)$ is rescaled as a Froude number $Fr(z) = \frac{\bar{V}(z)}{\sqrt{P(z)/\rho}}$, where $P(z)$ is the local confining pressure, a rescaling of all the flow curves is evidenced, for different intruder densities. This defines the so called ”mean flow rule” characterizing the intruder rheology. An important feature is that at large confining pressures, the intruder dynamics is intermittent and displays alternating phases of blockade and flow. The time spent in the blocked phase follows a statistics with a decaying power-law displaying an anomalous exponent around 1.5. This is quite reminiscent of the ”on-off” intermittency process [32] where the blocked phases show up with a similar residence time distribution, also evidenced for the flow out of a vibrated hopper [33]. We interpret the transition between blockade and flow as an effective friction threshold appearing as a ”noisy” generalization of the Coulomb threshold. When isolated, the dynamics of the flowing phases, displays a similar data collapse defining a ”dynamic flow rule”, however with a different functional form as for the ”mean flow rule”. Finally, for different intruder sizes, we could collapse both flow rules using a rescaled value of the Froude number increasing exponen-

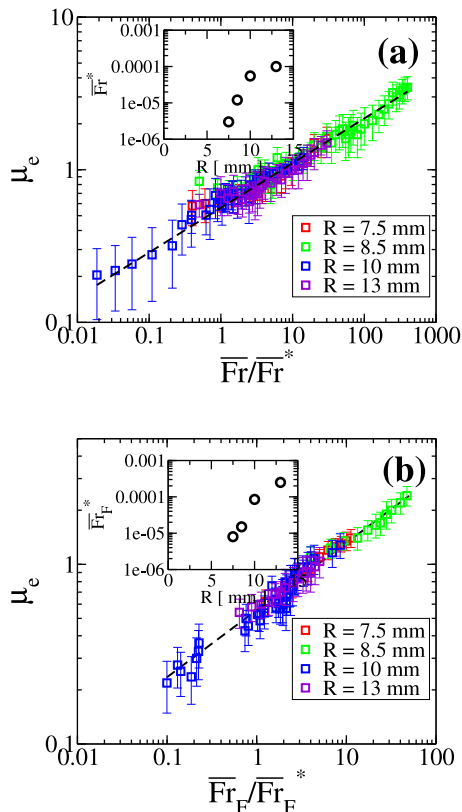


Fig. 7: (a) Mean flow rules for different intruder sizes represented as a function of a rescaled Froude number $\frac{\bar{Fr}}{\bar{Fr}_F^*}$ for different intruder radius R (fit $A_0 x^{A_1}$ with $A_0 = 0.56$ and $A_1 = 0.29$). Inset : rescaling Froude number \bar{Fr}_F^* as a function of the intruder radius. (b) Dynamical flow rules obtained in the flowing phase as a function of a rescaled Froude number $\frac{\bar{Fr}_F}{\bar{Fr}_F^*}$ (fit $A_0 x^{A_1}$ with $A_0 = 0.56$ and $A_1 = 0.37$). Inset : rescaling Froude number \bar{Fr}_F^* as a function of the intruder radius. Note the log scales for the vertical axis.

tially with the intruder size. We discuss the fact that this very strong dependance might be an indication that the effective rheology of the agitated packing is non-local.

Acknowledgement: We thank Bruno Andreotti for many scientific discussions and the CNES-2010 and ANR-2010-JamVibe programs for financial support.

REFERENCES

- [1] A. Liu, S.R. Nagel, Nature **396**, 21 (1998).
- [2] P. Habdas, D. Schaar, A. Levitt and E. Weeks, Europhys. Lett. **67**, 477 (2004).
- [3] S. Khan, C. Schnepper and R. Armstrong, J. Rheol. **32**, 69 (1988).
- [4] GDR Midi, Eur. Phys. J. E, **14**, 341 (2004); F. da Cruz, S. Emam, M. Prochnow, J.-N. Roux, and F. Chevoir, Phys.

- Rev. E **72**, 021309 (2005).
- [5] T.S. Majmudar, M. Sperl, S. Luding and R.P. Behringer, Phys. Rev. Lett. **98**, 058001 (2007).
- [6] A. Liu and S.R. Nagel (Editors), Jamming and rheology: Constrained Dynamics on Microscopic and Macroscopic Scales (Taylor & Francis, New York) 2001; L. Berthier and G. Biroli, Encyclopedia of Complexity and Systems Science (Springer, New York, 2008).
- [7] C. O'Hern, S. Langer, A. Liu and S.R. Nagel, Phys. Rev. Lett. **88**, 036001 (2002).
- [8] L. Bocquet, Phys. Rev. Lett. **103**, 036001 (2009).
- [9] S. Deboeuf, E. Lajeunesse, O. Dauchot, and B. Andreotti, Phys. Rev. Lett. **97**, 158303 (2006).
- [10] I. S. Aranson, L. S. Tsimring, F. Malloggi, and E. Clément, Phys. Rev. E, **78**, 031303 (2008).
- [11] J. J. Brey, M. J. Ruiz-Montero, and F. Moreno, Phys. Rev. E, **63** 061305, (2001).
- [12] H. A. Makse and J. Kurchan, Nature **415**, 614 (2002); F. Q. Potiguar and H. A. Makse, Eur. Phys. J. E, **19**, 171 (2006).
- [13] O. Zik, J. Stavans, and Y. Rabin, Europhys. Lett. **17**, 315 (1992).
- [14] G. D'Anna et al., Nature **424**, 909 (2003).
- [15] P. M. Reis, R. A. Ingale, and M. D. Shattuck. Phys. Rev. Lett., **98** 188301, (2007).
- [16] F. Lechenault, O. Dauchot, G. Biroli, and J. P. Bouchaud, Europhys. Lett., **83** 46003, (2008).
- [17] A. S. Keys, A. R. Abate, S. C. Glotzer and D. J. Durian, Nature Physics, **3** 260 (2007).
- [18] A. Cavagna, Physics Reports, **476**, 51 (2009).
- [19] G. A. Caballero and E. Clément, Eur. Phys. J. E, **30** 4 (2009).
- [20] K. A. Reddy, Y. Forterre, and O. Pouliquen, Phys. Rev. Lett. **106**, 108301 (2011).
- [21] K. Nichol et al., Phys. Rev. Lett. **104**, 078302 (2010).
- [22] R. Candelier and O. Dauchot, Phys. Rev. Lett. **103**, 128001 (2009).
- [23] A. Seguin, Y. Bertho, P. Gondret, and J. Crassous, *Dense granular flow around a penetrating object: Experiments and hydrodynamic model*, submitted (2011).
- [24] M.B. Hastings, C.J. Olson Reichhardt and C. Reichhardt, Phys. Rev. Lett. **90**, 098302 (2003)
- [25] R. Albert et al., Phys. Rev. Lett. **82**, 205 (1999); I. Albert et al., Phys. Rev. Lett. **84**, 5122 (2000).
- [26] J. Geng, R.P. Behringer, Phys. Rev. Lett. **93**, 238002 (2004); Phys. Rev. E **71**, 011302 (2005).
- [27] B. Dollet et al., Phys. Rev. E **71**, 013403 (2005).
- [28] P. Eshuis, K. van der Weele, D. van der Meer and D. Lohse, Phys. Rev. Lett. **95**, 258001 (2005).
- [29] M. F. Melhus, I. S. Aranson, D. Volfson, L. S. Tsimring, Phys. Rev. E **80**, 041305 (2009).
- [30] E. Clément, L. Vanel, J. Rajchenbach, J. Duran, Phys. Rev. E **53** 2972 (1996).
- [31] R. Harich, *Doctoral thesis*, University Pierre et Marie Curie (2010).
- [32] S. Aumaitre, K. Mallick and F. Petrelis, J. Stat. Phys., **123**, 909, (2006).
- [33] A. Janda *et al.*, Europhys Lett, **87**, 24002 (2009).